Journal of Theoretical and Applied Information Technology
15th July 2024. Vol.102. No. 13

ISSN: 1992-8645 www.jatit.org E-ISSN: 1817-3195

AUTOMATIC ROAD ROUGHNESS DETECTION AND RANKING USING DEEP LEARNING AND COMPUTER VISION

[1*]MUHAMMED SAFFARINI, [2]AMJAD RATTROOT, [3]YOUSEF-AWWAD DARAGHMI, [4]MUATH SABHA[*]

[1*]Faculty of Engineering and Information Technology, Arab American University, Jenin, Palestine

[2]Faculty of Engineering and Information Technology, Arab American University, Jenin, Palestine

[3]Computer Systems Engineering Department, Palestine Technical University-Kadoorie, Tulkarem, Palestine

[4]Faculty of Engineering and Information Technology, Arab American University, Jenin, Palestine

E-mail: [1]muhammed.saffarini@ptuk.edu.ps, [2]amjad.rattrout@aaup.edu, [3]y.awwad@ptuk.edu.ps, [4]muath.sabha@aaup.edu

ABSTRACT

Roads roughness is considered one of the most important problems that government institutions face because it requires many complex issues to find the roughness of the street. It also requires a lot of expensive tools which, in turn, measure the roughness of the roads. so, in this research paper we create a new model study road roughness and rank the roughness of this road automatically without the need for any cost or human intervention. Our proposed model checks the roughness by capturing the imaging using a drone, then it processes and analyzes the images coming from the drone, using several models that work together. our model shows the pattern of roads from the captured image using Gray level Size Zone Matrix(GLSZM) features Zone Percentage (ZP) and Size Zone Non-Uniformity (SZN) and then take the spikes of its distributions then take these spike to get optimal value K for Kmean to segment the image, the result of first model enter to second model that make sorting for this images depending on GLSZM features (ZP and SZV) to improve the result of our model, after that the image enter to CNN to get the outcomes by classifying it into which category this roughness belongs. The best accuracy we achieved in our model reached 91.94%, which is a very high accuracy, and therefore by a large percentage all correctly captured images from the drone has accurate results.

Keywords: *Computer Vision, Deep Learning, GLSZM, CNN, Road Roughness*

1. INTRODUCTION

The roughness of the pavement surface is the deviation of the road surface with respect to the original design surface. Road roughness affects ride quality, driver comfort, and safety [13]. Maintaining roads in good condition is necessary for reducing accidents probability, increasing driving comfort, and minimizing operational costs. Subsequently, roads condition should be monitored continuously to avoid roadway problems. Additionally, if road damage is discovered and maintained early, this will save governments expenses needed for maintenance [6]. Maintaining damaged roads in an early manner is 20% cheaper than repairing after the road is severely damaged [22]. To keep roadways in a proper condition, continuous monitoring and tracking of the pavement status is required. However, this is hard to be achieved manually, so automatic road surface roughness monitoring and ranking is required.

Detection of irregularities on the pavement surface, which is called pavement roughness, this is our problem that how to find the roughness of road in automatic way at minimal cost and effort, that the detection and get road roughness is necessary because damaged roads affect the riding quality and safety of the drivers. Also, early detection of damaged roads and rough pavements helps in reducing maintenance expenses and operational costs. Monitoring road conditions is hard to do manually, so many studies are conducted to automatically detect and evaluate road conditions.

One major indicator of the road quality is the road roughness.

To keep roadways in a proper condition, continuous monitoring and tracking of the pavement status are required. However, this is hard to be achieved manually, so automatic road surface monitoring is required.

The main problem that this paper is trying to solve is to find the roughness of the streets, in order to maintain the quality of the streets. We are looking into monitoring these streets to maintain their quality.

So, using Deep Learning and computer vision, we try to identify and classify street roughness using images taken using a drone

Therefore, this paper aims to find a way to classify, identify and ranking road roughness using deep learning techniques and computer vision techniques to recognize the roughness from road images and these images of the road taken using drones.

Then, we have created a new model that automatically finds roads roughness and classifies their degree of roughness using Convolution neural network and Gray level Size Zone Matrix (GLSZM) features. Our model is cost-effective and effective for monitoring road roughness.

To cover wide areas of the of region of roads, we used drones which are becoming popular these days due to low cost and high-quality images. Drones can transmit video streaming of roads to stations where the video can be stored and analyzed. To achieve high accuracy of video processing, we developed a new hybrid Deep Learning computer vision System consists of two model (one for selecting optimal K value using GLSZM features (ZP, SZV) and the second Sort Images before Entering CNN using GLSZM features distribution) to analyze road images and measure road roughness. The deep learning method should be able to fit with the accuracy that captured the roughness of roads at fine levels. Based on the roughness level that is used to rank roads according to [10], we ranked roads and suggest maintenance. so, from this point in this research we created a new model to overcome previous work problems. so, this paper contribution is:

1. build a new model that automatically detect roughness from images captured using drones (real streets), and measure its degree, rank roads based on the measured roughness degree depending in [10] to help municipalities keep automatically monitoring roads and reduce needed maintenance cost a study of pictures taken vertically without tilting from the drone
2. Develop new deep learning and computer vision model to automatically detect road roughness and measure roughness degree.
3. Our contribution that we create a new model consist of two models, the first one model tries to show the pattern of street from the captured image using GLSZM features Zone Percentage (ZP) and Size Zone Non-Uniformity (SZN) and then take the spikes of its distributions then take these spikes to get optimal value K for k-mean to segment the image.
4. And another contribution is made by result of the first model to the second model, that the second model make sorting for these images depending on GLSZM features (ZP and SZV) using goodness to fit technique in order to improve accuracy and reach higher performance, after that the image enter CNN to get the outcomes by classifying it into which category this roughness belongs
5. Depending on the roughness category, we will determine the quality of that road

One of the best applications for this model is road quality management applications for municipalities, as they no longer need to do this manually. Rather, all you need is to apply this model to images taken from a drone of any road belonging to this city, and this saves a lot of time, effort and cost, and from it you can monitor roads and determine if they need repair.

2. LITERAL REVIEW

Pavement surface roughness is the deviation of road surface with respect to the originally designed surface. One of the commonly used surface roughness measurements is the international roughness index IRI [20]. Road unevenness affects ride quality, driver comfort, and safety [26]. Maintaining roads in good condition is necessary for the development of governments economics. So, road conditions should be continuously monitored to avoid road problems. Additionally, if road devastation is discovered and maintained early before it grows, this will save governments a lot of costs and expenses needed for maintenance [6]. The authors of [27] show that the cost of maintaining damaged roads early is 20% less than that of repair

after the road becomes heavily damaged. The development of road roughness detection techniques has been divided into three categories depending on the type of data to be processed to detect road surface roughness accelerometer-based, image-based, laser-based, and friction noise approaches.

2.1 Accelerometer based approaches

Different systems were developed to study road conditions using road roughness measurement using different tools. The accelerometer is one of the most widely used tools for reading roughness data. Accelerometer data have been used for pavement roughness detection. Accelerometer signals are collected, analyzed, and then the roughness degree is calculated. Different types of accelerometers were used, such as: Stand-alone, smartphone, and other types of accelerometers.

2.1.1 Standalone accelerometer

Boltzmann machine deep neural network algorithm based on the Ada boost Backward Propagation algorithm used in [22] to determine rough regions of the roads. The input to this network is the vertical vibration power spectrum which is divided into two categories: high and low frequency vibrations. Low frequencies are the one resulted because of the roughness of the road. The Boltzmann network classifies these signals and vibrations and recognizes the rough regions of the road. while in [29] authors intended to exactly determine the location of critical roughness values of road pavement. The aim of such a study is to determine roads that need emergency maintenance. The results are directed at municipalities to prioritize the maintenance process of roads. Roughness data with 10 m intervals were collected on a 3140 m divided road using a smartphone. The collected data were analyzed using the distance-dependent Mann-Kendall trend analysis method and checkerboard model. A novel machine learning approach was developed for the detection of road roughness in [4] by calculating the international roughness index IRI by analyzing the acceleration z-axis and varying the speed of the car recorded by an in-car sensor. Data preprocessing includes map matching of vehicle path to the OSM network based on HMM model. OSRM service and segment alignment using the data from the GPS sensor were used for implementation. After that, the feature vector of 68 features were extracted, but only 38 features were used for roughness detection. Then, using a set of machine learning models, the roughness index was calculated. Finally, IRI index was used for studying the significance of "Road Levelling Project" in the New Taipei city by the government in [8]. The International Roughness Index IRI of 152 asphalt concrete pavement sections in New Taipei city was collected before and after the road leveling project for this task. A mechanized profilograph expressed by the profile index PI was used to measure the roughness of roads. The PI ranges between 0 (Grade A) and 5 (Grade E) (roughest to smoothest) and its unit is meters/meter. In fact, PI and IRI are related as shown in [21]. Also, from [9] the relation between the Pavement Riding Quality Index (PRQI) and IRI was shown.

2.1.2 Smartphone accelerometer

Several approaches used smartphones accelerometer as an easily available alternative for reading road acceleration signals for road roughness detection and estimation as in [18][2] [17] [32][5][1]. In [18] CNN was used to obtain road roughness data from raw time-history measurements obtained from vehicle responses. A CNN model was trained for the international roughness index estimation regardless of the types of vehicles and driving speed. A huge data set was created using half-car simulation with 31-km road IRI information, actual driving speed profile and corresponding accelerations, angular velocities. Four types of vehicles, 60 distinct vehicle models; and 16 driving speeds were used for CNN architecture training, validation, and testing. The impact of road roughness on vehicle speed is studied in [1] by the use of Android application called Roadroid Pro, which computes road roughness in terms of two values estimated IRI which depends on peak value and root mean square vibration at speed between 20-100 km/h. while calculated IRI computed at speed between 60-80 km/h. from these measurements' authors concluded that there is a significant impact of road roughness on vehicle speeds in peak hours. Finally, in [5] an approach is developed to distinguish paved and unpaved roads, then anomalies are detected on paved roads. This is done by developing an Android application that reads values from four sensors accelerometers (x, y, z), tri- axial gyroscope (x, y, z), three points of GPS (latitude, longitude, altitude), and compass. The collected data were preprocessed and a feature vector of 130 features is extracted. Features vectors are used as an input to SVM, HMM and ResNet classifiers to classify paved and unpaved roads. Finally, for paved roads, the Y filter is applied, and then KNN and DWT classifier were used to detect

road anomalies. Another research used accelerometers built in smartphones such as [2][17][32][5][1]. The results of the studies are analyzed and compared.

2.2 Vision-based approaches

As mentioned above different tools were used to collect data of roads for roughness detection and classification. The first one is accelerometers which were discussed in the previous section. Another type of road data is road images that are used to extract road features and estimate pavement roughness. Road images can be collected using different types of cameras as videos or static images.

2.2.1 Stored video-based methods

Videos of pavement are recorded using a camera placed at the rear of a vehicle in [15]. Frames and their geospatial locations are extracted from these videos, converted into grayscale, then enhancements are conducted to remove blur, shadows, and inconsistencies in image colors. Consequently, image entropy value is computed. Depending on the entropy value images are classified to healthy pavement or distressed pavement, if the entropy value is less than a pre-defined threshold then the pavement is distressed. Finally, a heatmap of the distressed pavement regions is created. Videos of pavement surface were recorded using a camera put at the rear of the vehicle. 21600 frames were extracted from these videos such that 8423 are images of distressed pavements and 13177 images are healthy pavements. Images were preprocessed, entropy valued were calculated, then pavements were classified as healthy or distressed pavements accuracy, precision, recall and F1 score of 89.2%, 86.6%, 85.6%, 18 and 86.1%, respectively were achieved.

2.2.2 Static images-based methods

Several pavement roughness detection and classification used static images taken by camera or from a predefined dataset as [33][12][31][16][23][13][14][7][11][30] A vision-based technique to detect rough roads was proposed in [33]. Two methods were proposed to estimate concrete surface roughness quantitatively from images. The first one is a digital image processing technique developed to classify coarse aggregate from cement paste. They depend on the image color to achieve this task, by taking in consideration that the aggregate is lighter in color than the cement, so these differences in color is used to measure the roughness of the concrete surface as the coarse aggregate areas increased the roughness of the concrete surface increased. This method works as follows: first the prepare the images, enhance them, convert them to grayscale, and finally, the images are binarized to become black and white images. White regions represent the aggregate and black regions represent the cement. The ratio of the aggregate area-to-the total surface area can be used as an indicator of surface roughness. And there is another research like [25] this research based on GLCM and CNN to get the pattern of the texture and then classify it, in our paper, we have studied street roughness from another perspective and other techniques that this research studied it from the perspective of repeating adjacent values using GLCM to find the value of K for Kmean while in our new research paper, we have studied the points connected to each other using GLSZM to find the optimal K and make improvement on CNN using also GLSZM, in order to improve accuracy and reach higher performance.

2.3 Laser-based approaches

Another way of roughness detection is to use laser scanning as in [19] where an automated algorithm is proposed for detecting road roughness from Mobile Laser Scanning data. The algorithm goes through several steps as follows:

1. Road boundary is coated on the LiDAR data to remove the points outside the road boundary and save the inner points to estimate the road surface.
2. The LiDAR cloud points are inserted into intensity raster surface to ensure a more computationally efficient method for road roughness detection, and point thinning process is applied to reduce the noise of the surface.
3. In the next step, three-level Otsu thresholding is applied to detect the candidate roughness regions from the raster surface.
4. The Lidar points of the detected regions are clustered. These clusters are filtered then to remove noises and outliers.
5. Finally, the resulting LiDAR points are then finally rotated back to their original position on the road.

Furthermore in [24] authors used both laser scanner and accelerometer to study the roughness of

several roads and the effect of roughness on vehicle stability. They studied the applicability of Kinect depth camera to measure roughness parameters of 4 different forest unpaved roads and one asphalt road that was considered as a reference. The Kinect depth camera sends infrared pattern onto the road surface, then the reflected light pattern from the road surface is collected and compared with the initial pattern to create the disparity map which in turn is used to reconstruct 3D road surface, and the collected depth scans is used to calculate the quantitative roughness parameters. They also used an accelerometer sensor to read 3-axis acceleration values and calculate the correlation between the car vibrations and the roughness of the road, to study the stability of different vehicles corresponding to the roughness of that road.

2.4 Tire/road friction noise-based approach

Researcher in [28] proposed another approach to detect asphalt problems by analyzing the noise sound resulted from the friction between tire and road. They first recorded the noise from the interaction between the tire and the asphalt. The acoustic signal was sampled at 51 kHz, and framed in 100ms without overlapping, after that the 1/3-octave filter bank is applied on the signal. From these signals a dataset of 23590 instances is created. Finally, KNN classifier with K=3 was used for pattern recognition to study the asphalt condition.

3. METHODOLGY

In this research, the road roughness is to be calculated using drone images. These images are used to extract surface texture. These textures are then classified using deep learning models and computer vision algorithms. Gray Level Size Zone Matrix (GLSZM) is generated, and different operations are performed to extract different features of the road. Since many sophisticated classifiers exist, the key challenge here is the development of effective features to extract from a given textured image. texture is classified strictly based on a set of small patches of pixels extracted from a given textured image. There are many methods to get the perform this task; including histogram properties, local binary descriptor (LBD), k-means and graph theory. The developed model is based on Hybrid principle. Several stages study different aspects of on the problem then collaborate in the decision-making process. The model consists of several stages, as each stage can work separately and show results, but when they are combined, it shows excellent results. Each stage processes the given images in a different way to get the road roughness classification. The result from each stage is then sent to the final model to decide on the road roughness classification.

3.1 Image acquisition (drone, collection, resolution, dataset, samples)

A camera can be installed in a number of places on a moving vehicle, including the dashboard, the back, and the front. The photos obtained from these places, however, tend to be skewed and take a long time to cover city streets. In order to get around these problems, a drone is employed in this study. As the drone may be set to cover city roads when there is little traffic and adequate lighting, this is possible. a DJI MAVIC air 2 drone is utilized. A 12" CMOS camera sensor with a 48MP resolution and a FOV of 84O is included with the drone. This drone can record videos at a frame rate of 60 frames per second in 4k (3840x2160). Also, the drone has optical image stabilization, and it is programmed to withstand wind.

3.2 Preprocessing

The videos are recorded in.mp4 format at a resolution of 4k x 60 frames per second. The picture dataset is created by selecting two frames at random from the video footage that was recorded. The films were taken twice, once around midday and once in the late afternoon. This takes into account the various daytime illumination situations. Gamma correlation is used to standardize the lighting for photos taken throughout the day. Gamma of 0.8 is applied to images that are taken at midday (i.e., in decent lighting). And the photos taken later in the afternoon are given a gamma of 1.5. As shown in the *Figure **1*** and *Figure **2***

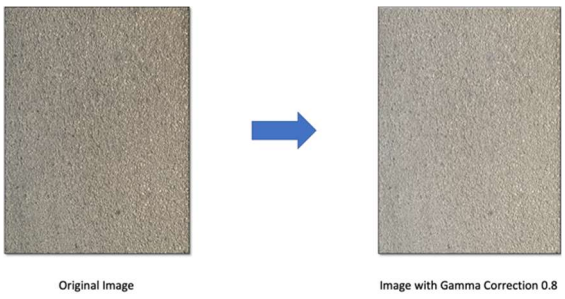

Figure 1 Original Image Vs. Image with Gamma Correction 0.8

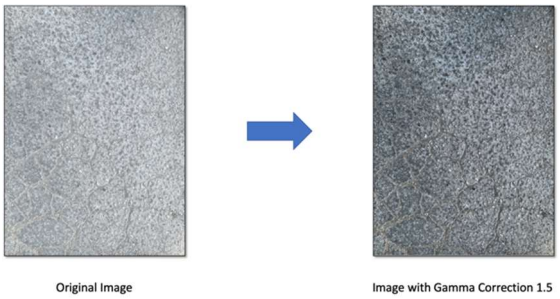

Figure 2 Original Image Vs. Image with Gamma Correction 1.5

Gaussian blur is further used to reduce picture noise. The standard deviation value for this filter is 5 in both directions (x and y). As shown in the following *Figure **3***

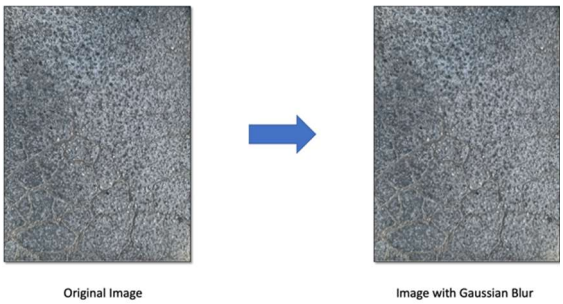

Figure 3 Original Image Vs. Image with Gaussian Blur 5

3.3 Our Model (RRGSK)

The first stage studies images distributions and determines the number of spikes in these distributions, these spikes mean that there is a certain concentration of the data inside the image, that is, it works to determine the distinctive pattern inside the image. This value is then reduced and used as a k value in the k-means algorithm, then the resulting images are ordered using the second stage. In the second stage, images are ordered automatically using the GLSZM features and its distributions before training the CNN. This enhances the prediction accuracy of the classification and it's used to train CNN model as shown in *Figure **4***.

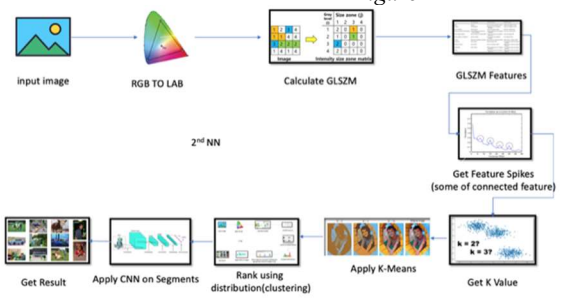

Figure 4 Our Workflow of The Whole Model RRGSK

RRGSK is Composed of Two stages:

1. First Stage is Key Feature Determine.
2. Second Stage is Ranking Images and Classification.

3.3.1 Key Feature Determine Stage

As shown in the first 5 steps ***Figure 4***. This model is developed to detect key features in the image and remove other less important features such as noise and unneeded information and ...etc. In our method, we relied on CLSZM (Gray Level Size Zone Matrix), which used to measure areas of adjacent pixels in the image, which in turn contains a set of properties that describe the image. At the beginning we take an image from the data set, but here we did not deal with images in the RGB system, but rather we converted the image from the RGB system to LAB, because LAB has a large space and a larger range of colors Much of the RGB system as shown in *Figure **5***.

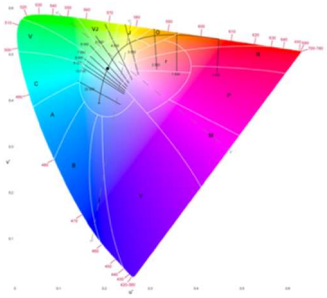

Figure 5 LAB Color Space

After the image is converted to the LAB color space, each layer is taken separately and the GLSZM is calculated for each layer. GLSZM matrix is calculated for each layer in the LAB space and used to quantify regions of contiguous pixels in the image. The LAB space consists of three layers. The L layer, which stands for lightness ranges from 0-100. The A layer, which quantifies the change from red to green, where red has negative values and green has positive values. And the B layer, which quantifies the change from negative values for yellow to positive values of blue. The difference between blacks and grays in an image is represented by lightness. A and B are multicolored, displaying every unit in contrast to its corresponding color.

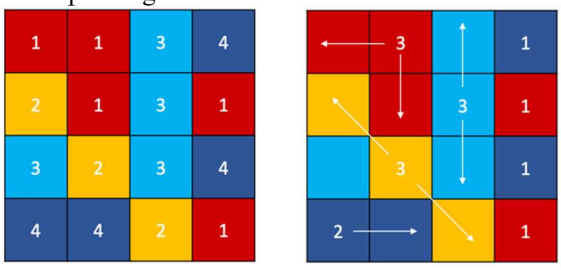

Figure 6 GLSZM Matrix

The calculated matrix shown in *Figure* ***6*** is made up of several colors. Each color is linked to all its lengths, i.e. the cyan color in the figure has two lengths 1 and 3. Additionally, the length repetition of each color is also recorded. The average matrix is then calculated for the feature matrix of all three layers, then distributions for these features are plotted. Several features can be calculated from the GLSZM matrix the **SZV**, and **ZP** that indicate for rough in high value or smooth in low value are used in this model. **SZN** evaluates the variance of size region volumes in a picture, with a lower amount suggesting greater size zone volume homogeneity. the equation of **SZN in equation (1) [34]** is

$$SZN = \frac{\sum_{j=1}^{N_s}\left(\sum_{i=1}^{N_g} P(i,j)\right)^2}{N_z} \quad (1)$$

Where the N_S is the number of discreet zone sizes in the image, N_g is the number of discrete intensity values in the image, N_Z is the number of zones in the image and the p(i,j) is the values inside normalized size zone matrix.

ZP calculates the roughness of the texture by dividing the number of regions by the number of coordinates in the ROI. The equation of ZP **in equation (2) [34]** is:

$$ZP = \frac{N_z}{N_p} \quad (2)$$

where N_P is the number of pixels in the image, and N_Z is the number of zones in the image, and the p(i, j) is the values inside normalized size zone matrix.

The number of spikes in each feature distribution is calculated and plotted as shown in figures Figure 7 , Figure 8, which represents the extent of data concentration in places and the extent of its decrease in places.

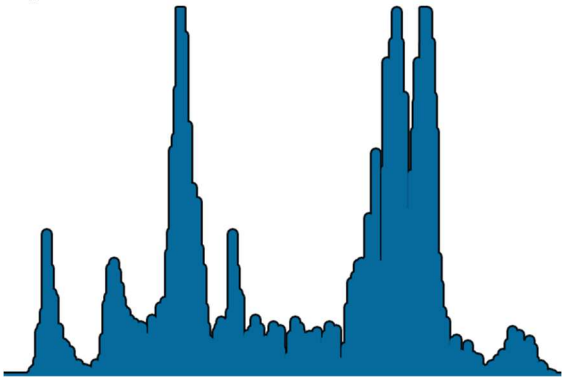

Figure 7 Distribution Of ZP

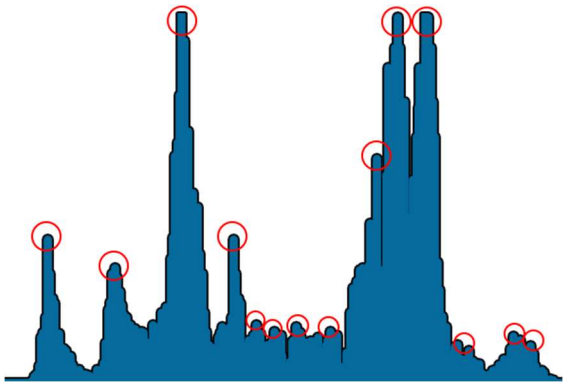

Figure 8 Determine The Spikes In ZP Distribution

Here in *Figure* ***8***, these spikes symbolize that at each one there is a certain focus of the data and texture inside the image, and this focus symbolizes the pattern that this image contains, and that is why we want here to study this pattern.

We propose Calculating the K values directly from taking the average of these two values (# spike for ZP and SZV) as

$$K = \frac{SZV_{spikes} + FZP_{spikes}}{2} \quad (3)$$

where SZV_{spikes} is the number of spikes in SZV distribution, and ZP_{spikes} number of spikes in ZP distribution.

The outcomes from this equation yield high K-values. This means higher number of clusters for the K-mean clustering. As shown in *Figure* ***9***

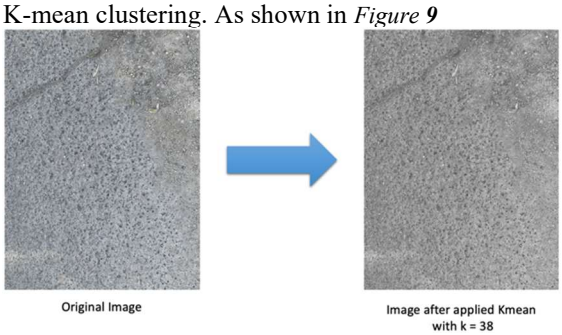

Figure 9 Image After Applying K-Means Using GLSZM With High Value Of K = 38

And since only the key features need to be extracted, lower K-values need to be used. Therefore, FreeDman-Diaconis rule [35] is utilized to calculate the less value of K-value using equation 4,5 [35]. which makes it very robust compared with calculating the K-value directly which will not yield usable results.

$$K = 2 \times \frac{IQR}{\sqrt[3]{N}} \quad (4)$$

$$IQR = Q2 - Q1 \quad (5)$$

Where: IQR is the interquartile of the values inside the vector, n is the number of values, Q1 is the first

quartile of the values inside the vector, and Q3 is the third quartile of the values within the vector.
The average K-value for the SZV and ZP features is calculated and used as the number of clusters that we want to apply in K-means.
From that we calculate the Freedman-Diaconis rule SZV for ZP, we then calculate the average for the value between the result of Freedman- Diaconis rule for SZV values and the result of Freedman- Diaconis rule for ZP values. Then apply the Freedman-Diaconis rule in SZV using

$$IQR_{SZV} = Q3_{SZV} - Q1_{SZV} \quad (6)$$

$$K_{SZV} = 2 \times \frac{IQR_{SZV}}{\sqrt[3]{N_{SZV}}} \quad (7)$$

Where: $Q1_{SZV}$ is the first quartile of the values inside SZV vector, $Q3_{SZV}$ is the third quartile of the values inside SZV vector, IQR_{SZV} is the Inter-quartile of the values inside SZV vector, and N_{SZV} is the number of values inside SZV vector.
then for applying the Freedman-Diaconis rule in ZP using equation 8

$$IQR_{ZP} = Q3_{ZP} - Q1_{ZP} \quad (9)$$

$$K_{ZP} = 2 \times \frac{IQR_{ZP}}{\sqrt[3]{N_{ZP}}} \quad (10)$$

Where: $Q1_{ZP}$ is the first quartile of the values inside the ZP vector, $Q3_{ZP}$ is the third quartile of the values inside the ZP vector, IQR_{ZP} is the Inter-quartile of the values inside the ZP vector, and N_{ZP} is the number of values inside the ZP vector.
Then the final k is to take the average between K_{SZV} and K_{ZP} as in this equation

$$K = \frac{K_{SZV} + K_{ZP}}{2} \quad (11)$$

Where: K_{SZV} is Freedman- Diaconis for SZV, and K_{ZP} is Freedman- Diaconis for ZP
The resulting image has fewer colors with a clear pattern. Hence, only the key feature with higher power comes into the picture. Other features such as noise are less important to the data. will not be in the image as shown in *Figure **10***

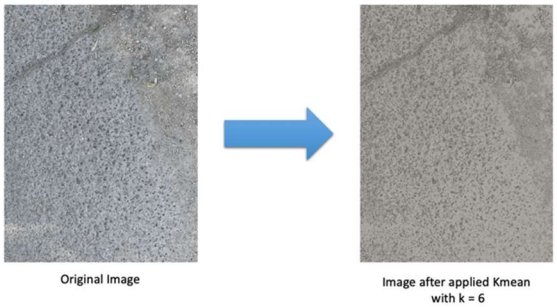

Figure 10 Image After Applying Kmean Using GLSZM With K = 6

After that, the images are rearranged using the second stage called" Ranking Images and Classification Stage". This is done since *Figure **4*** before entering the images to CNN. Then these images are then used to train the CNN model.

3.3.2 Ranking Images and Classification Stage

There are several types of CNN, and each one has its own characteristics and specifications. These types are distinguished in the modification of the convolution stage. Some of them add stages to the filter or modify the way they are arranged, but we have made a new idea, which is how to enter the images into the convolution stage, where we found the way the images are entered and the way they are arranged. It has a significant effect on the accuracy of the model, so we created a new way to make a certain arrangement of how the input images are distributed in the CNN model. In this model, road images are ordered on the basis of their GLSZM features and distributions. Ordering the images gives CNN the opportunity to grow and learn rather than giving the network random images.

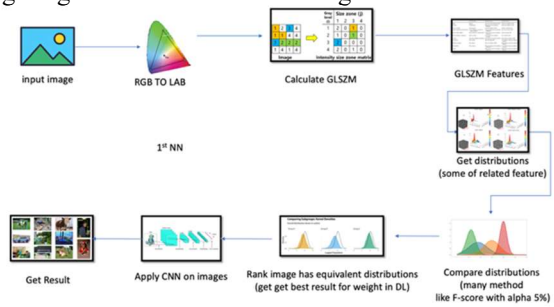

Figure 11 Our Model For Ranking Images And Classification Stage

As shown in Figure 11, which represents our model for this stage, the input to this stage is the Key Feature Determine stage, the same process utilized in the first stage is done in this model. That is, the system is first converted into the LAB space, then the GLSZM is generated. After that, the SZV and ZP feature vectors are calculated for each layer in the LAB space. Then the average, for the three layers in the LAB space, then distributions for these features are plotted. In our method, we relied on CLSZM (Gray Level Size Zone Matrix), which used to measure areas of adjacent pixels in the image, which in turn contains a set of properties that describe the image, so we used these properties in order to find (the nearest or farthest image in the dataset) through the distribution of these properties and compared with the distribution with the rest of the images using Kolmogorov-Smirnov test [36].This matrix has several features that describe the image. The distribution of these features for each image is generated. Then the Kolmogorov-Smirnov test was used to compare these distributions to find the

nearest and farthest image in the dataset using equation (12)

$$KS = Maximum|F_{n1} - F_{n2}| \quad (12)$$

Where ks is the value of Kolmogorov-Smirnov test, n1 is Observations for first Distribution. n2 is Observations For second Distribution, and the two distributions in cumulative distributions

Several features can be calculated from the GLSZM matrix the **SZV**, and **ZP** (that indicate rough in (high value) or low roughness in (low value)) are used in this model. **SZN** or **SZV** evaluates the variance of size region volumes in a picture, with a lower amount suggesting greater size zone volume homogeneity. **ZP** calculates the roughness of the texture by dividing the number of regions by the number of coordinates in the ROI. Vectors of these features are generated. And the distribution for these vectors is plotted. As shown in Figure 12

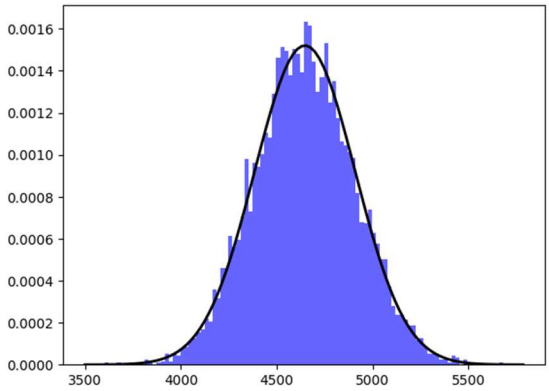

Figure 12 Zp Vector Distribution

The cumulative distribution for each image, shown in *Figure* ***13*** (for each feature) has compared them with the distribution for all other images in the dataset using the Kolmogorov-Smirnov test (or goodness of fit). In this test, any two distributions can be tested whether they belong to the same distribution or to different distributions. This is done by calculating the maximum distance between the two distributions (D) as shown by equation 12. The lower the value of **D**, the more similar the distributions, and vice versa.

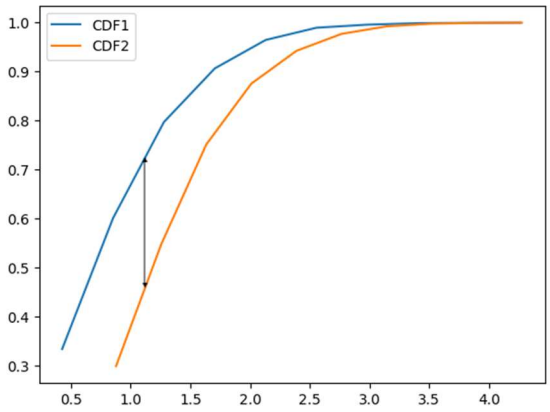

Figure 13 Cumulative Distribution For Two ZP Distributions

$$\mathbf{D_{ZP} = Maximum|FZP_{n1} - FZP_{n2}|} \quad (13)$$

where is FZP_{n1} is Observations for the first image distribution in cumulative distributions, FZP_{n2} is Observations For second image Distribution in cumulative distributions, And the two distributions in cumulative distributions, and D_{ZP} is maximum distance between two ZP distributions.

It has been observed that when the cumulative distributions show a significant deviation **D**, It denotes the difference among the two distributions. Then the same process is applied to the SZV feature as fallowing equation

$$D_{SZV} = Maximum|FSZV_{n1} - FSZV_{n2}| \quad (14)$$

where $FSZV_{n1}$ is Observations for the first image distribution in cumulative distributions. $FSZV_{n2}$ is Observations for second image Distribution in cumulative distributions (both distributions in cumulative distributions) and DSZV is maximum distance between two SZV distributions.

It has been observed that when the cumulative distributions show a significant most deviation **D.** It denotes the difference among the two distributions. After that, the averages of these D_{ZP} and D_{SZV} are calculated as shown in equation 14

$$D = \frac{D_{ZP} + D_{SZV}}{2} \quad (15)$$

Where: D_{ZP} is maximum distance between two ZP distributions and D_{SZV} is maximum distance between two SZV distributions.

All images are then ordered ascending based on the distance between their distributions using value deviation as in *Figure* ***14*** and then the ordered images are used to train the CNN model.

Journal of Theoretical and Applied Information Technology
15th July 2024. Vol.102. No. 13

ISSN: 1992-8645 www.jatit.org E-ISSN: 1817-3195

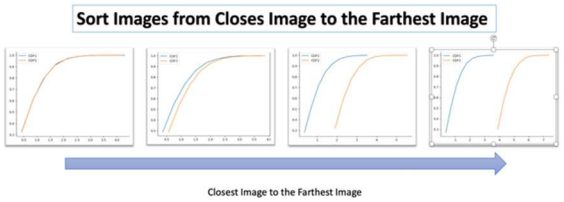

Figure 14 Sort Images From Closes Image To The Farthest Image

4. Experiments and Result

We used the Google platform, Colab, which in turn provides us with high-quality servers and resources to process and write our model , the specification of our version of colab is RAM 12.7 GB , HD 107 GB and for processing we use T4 GPU, this help us to solve the complexity of size of captured images and the complexity of processing the high resolution of images .

4.1 Dataset

In this research, a new dataset is created. Roads scattered along Tulkarm city in Palestine, with different conditions ranging from excellent to very poor are studied. Videos are captured using DJI Mavic air 2 drones with 3840x2160 (4K) resolution. 1500 videos with total runtime of 1500 are recorded. These videos cover 150 KM road length.

From these videos a total of 15326 images are extracted. These images are in the same resolution as the videos as shown in *Figure **15***. These images are then pre-processed to enhance lighting and remove noise using gamma correlation and blur filters, respectively. as shown in *Figure **15***

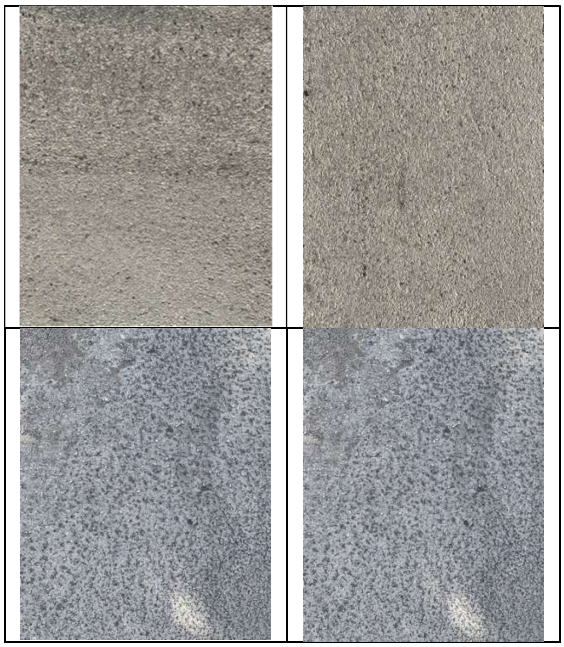

Figure 15 The Roads With Different Roughness Ranking From Degree1 To Degree 6 Respectively

4.2 Result of RRSGK Model

show the Result of the Whole Neural Network Model, which is represented in *Figure **4***, as we said earlier in the previous section, this Neural Network relies on two stages. The first is that it selects certain features of GLSZM and relies on its distribution in order to determine the value of K that will be entered into Kmean in order to show the pattern of the image and hide unnecessary details from the image, as shown in *Figure **16***

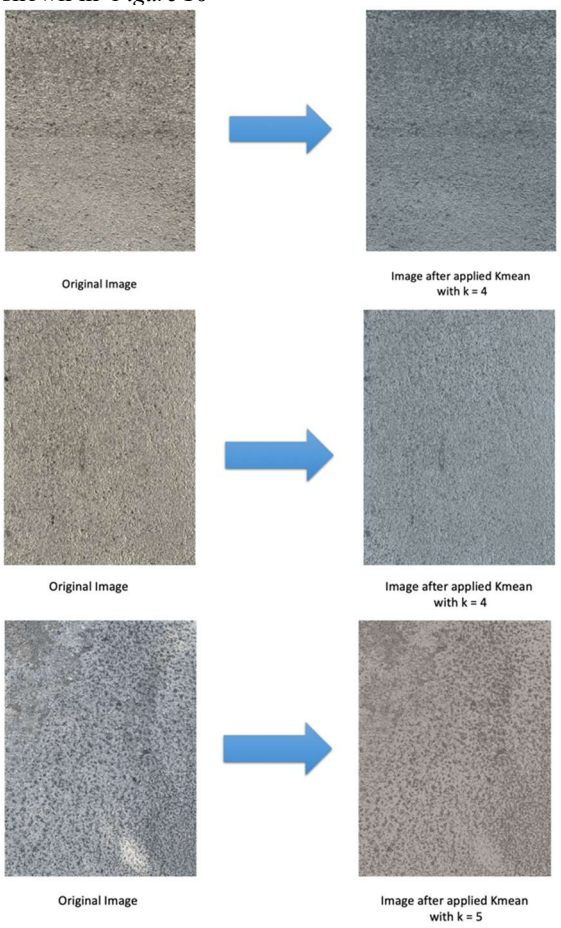

Journal of Theoretical and Applied Information Technology
15th July 2024. Vol.102. No. 13

ISSN: 1992-8645 www.jatit.org E-ISSN: 1817-3195

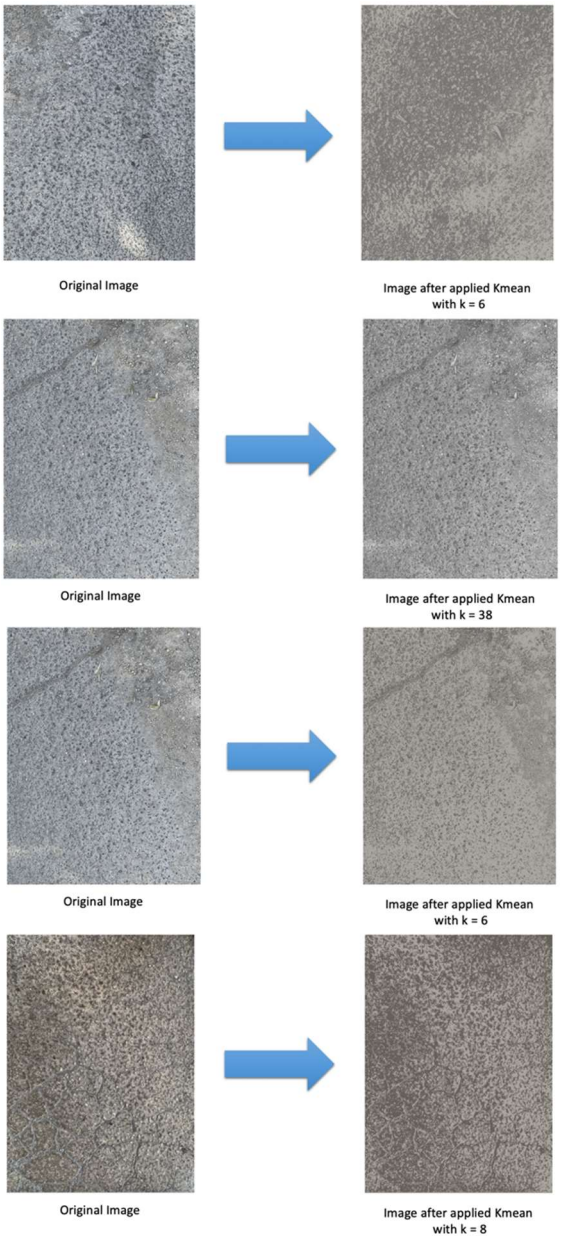

Figure 16 The Roads With Different Roughness With Different K For K Mean Ranking From Degree1 To Degree 6 Respectively

The second stage is sorting the images before entering the Neural Network (ascending or descending) by using the f-score that was calculated by calculating the distribution through the features of GLASZM.

In the beginning, we calculated the results for (VGG16) Neural Network without using the proposed method.

Table 1 Result Of Default VGG16 Model

Class	Accuracy	Precision	Recall	F1-score
R1	80.96%	0.809	0.80019	0.80457
R2	80.30%	0.789	0.81019	0.799454
R3	78.88%	0.819	0.81019	0.814571
R4	78.47%	0.789	0.81019	0.799454
R5	80.16%	0.7975	0.80869	0.803056
R6	80.96%	0.786	0.80319	0.794502
AVG	79.96%	79.83%	80.71%	80.26%

As shown in default VGG16 model outcomes *Table **1***, and then we used the aforementioned method and showed the results related to the classifications, and the results of the classifications appeared as follows for the 6 classes, which are the degrees of roughness present In [10] Accuracy, Precision and Recall were calculated for each class separately, and the f-score was calculated for them as shown in the following *Table **2***:

Table 2 Result Of Our Whole Mode (RRGSK)

Class	Accuracy	Precision	Recall	F1-score
R1	92.91%	0.936	**0.951**	**0.9434403**
R2	91.94%	0.9301	0.943	0.9365055
R3	90.83%	0.926	0.938	0.9319613
R4	90.42%	0.914	0.917	0.9154975
R5	91.64%	0.916	0.935	0.9254024
R6	**93.91%**	**0.943**	0.913	0.9277575
AVG	91.94%	92.75%	93.28%	93.01%

As shown in the previous *Table 2*, the highest accuracy was for class No. 6, which is the class that symbolizes the roughest streets with an accuracy of 93.91\%, and the least accurate is class No. 4 with a value of 90.42\%, which symbolizes a fourth-degree roughness according to the roughness standard of [10]. As we can see from the previous *Table 2* the results were of high values compared to default model and from it we conclude that this neural network has achieved what is required, which is that the process of showing features and patterns within the images through the use of k-means and finding the best value for K through the distribution of the GLSZM properties and arranging the images in a way ascending had a very positive effect on the accuracy results in Neural Network, by preserving the shape of the weight change that exists within the network, as the combination of the two methods with

each other led to better results than the default model.

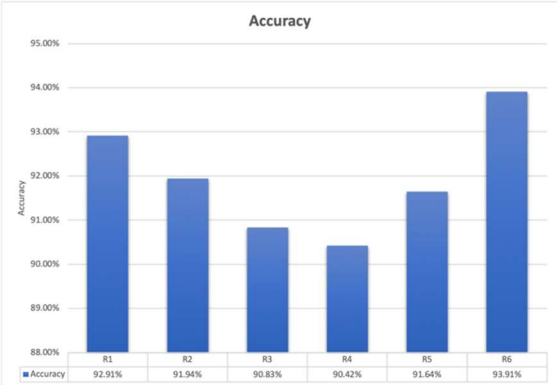

Figure 17Our Model Accuracy For All Roughness Classes

As shown in the *Figure 17*, our whole model has shown very strong results in classification the degree of roughness, as all the classes were classified with an accuracy of more than 90%, especially in classify the most rough class, which is class No. 6, with a result of 93.91%, and the mid roughness class No. 4 is the lowest accuracy with 90.42%.

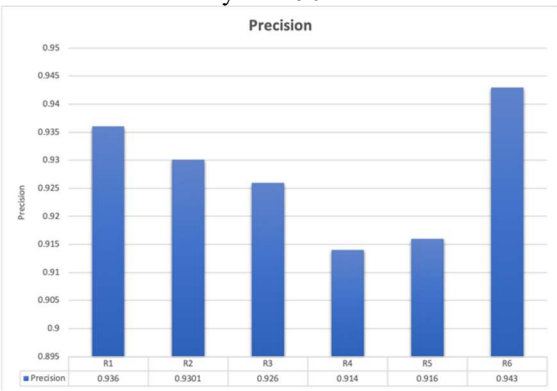

Figure 18Our Model Precision For All Roughness Classes

As shown in the *Figure 18*, our whole model has shown very strong results in get precision in retrieve the degree of roughness, as all the classes were retrieve with an precision of more than 91%, especially in classify the rough class, which is class No. 6, with a result of 94.3%, and the mid roughness class No. 4 is the lowest accuracy with 91.4%.

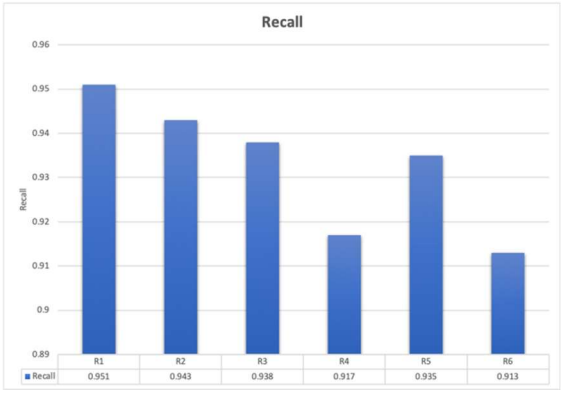

Figure 19 Our Model Recall For All Roughness Classes

As shown in the *Figure 19*, our whole model has shown very strong results in get recall in relevant degree of roughness, as all the classes were classify with an recall of more than 91%, especially in classify the less rough class, which is class No. 1, with a result of 95.1%, and the most roughness class No. 4 is the lowest recall with 91.4%.

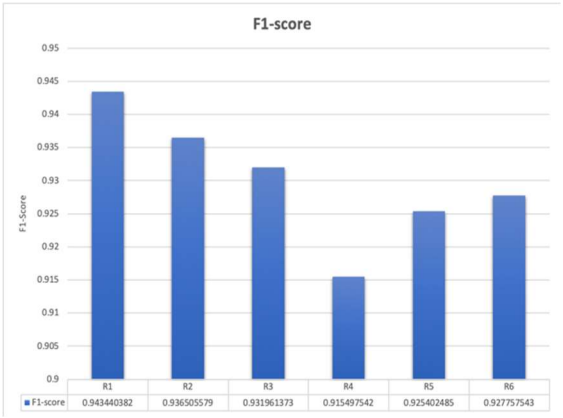

Figure 20 Our Model F1- Score For All Roughness Classes

As shown in the *Figure 20*, our whole model has shown very strong results in F1-Score of get degree of roughness, as all the classes were classified with an f1-score of more than 91.5%, especially in classify the less rough class, which is class No. 1, with a result of 94.3%, and the mid roughness class No. 4 is the lowest accuracy with 91.5%.

4.3 Result of Our Model Without using Our Ranking

Table 3 Result Of Our Model Without Using Our Proposed Sorting Images Method

class	Accuracy	Precision	Recall	F1-score
R1	89.41%	0.892	**0.907**	**0.899437**
R2	88.44%	0.8861	0.899	0.892503

R3	87.33%	0.882	0.894	0.887959
R4	86.92%	0.87	0.873	0.871497
R5	88.14%	0.872	0.891	0.881397
R6	**89.51%**	**0.899**	0.869	0.883745
AVG	88.29%	88.35%	88.88%	88.61%

As shown in the *Table* ***3***, the model that relies on showing the pattern without sorting the images showed good results, regardless that with the sorting of the images there is a difference in the results as with the sorting of the images, the results of all classes almost exceed 87\% in terms of accuracy, but here it has decreased from 90\%, and this is great evidence that the sorting of images in the classification process is very important and our proposed method in sorting is powerful. Although, if we look at the results in terms of accuracy, the results were somewhat high. The roughest class achieved a result of approximately 90% which is 89.5\%, and this is evidence that the model is able to classify the image correctly.

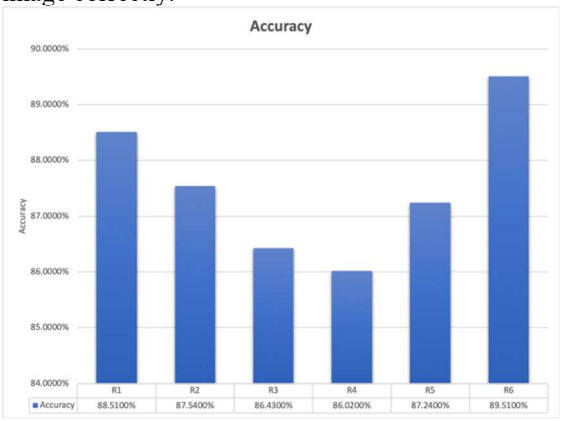

Figure 21 Our Model Without Our Sorting Accuracy For All Roughness Classes

As shown in the *Figure* ***21***, our sub model of showing the pattern without sorting the images has shown very strong results in classification the degree of roughness, as all the classes were classify with an accuracy of more than 87%, especially in classify the most rough class, which is class No. 6, with a result of 89.51% it almost 90%, and the lowest value is class No. 4 Accuracy 86.92% it almost to 87%

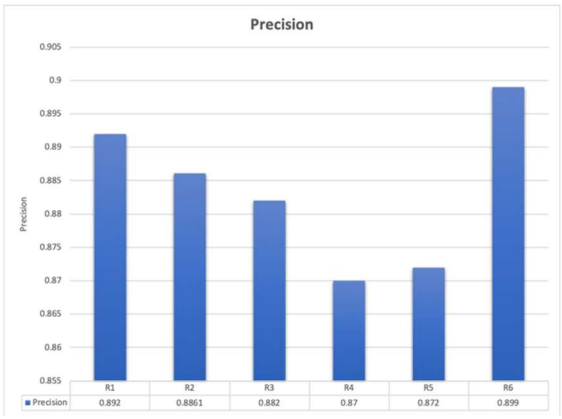

Figure 22 Our Model Without Our Sorting Precision For All Roughness Classes

As shown in the *Figure* ***22***, our sub model of showing the pattern without sorting the images has shown very strong results in get precision in relevant degree of roughness , as all the classes were retrieve with an precision of almost is over 87%, especially in classify the rough class, which is class No. 1, with a result of 89.9% it almost 90%, and the lowest value is class No. 4 with precision value is 87%.

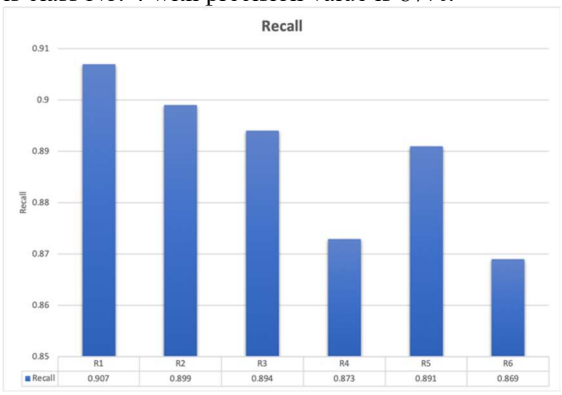

Figure 23 Our Model Without Our Sorting Recall For All Roughness Classes

As shown in the *Figure* ***23***, our sub model of showing the pattern without sorting the images has shown very strong results in get Recall in retrieve the degree of roughness, as all the classes were retrieve with an Recall of almost is over 87%, especially in classify the lowest rough class, which is class No. 1, with a result of 90.7%, and the lowest value is class No. 6 with Recall value is 86.9%.

Journal of Theoretical and Applied Information Technology
15th July 2024. Vol.102. No. 13

ISSN: 1992-8645 www.jatit.org E-ISSN: 1817-3195

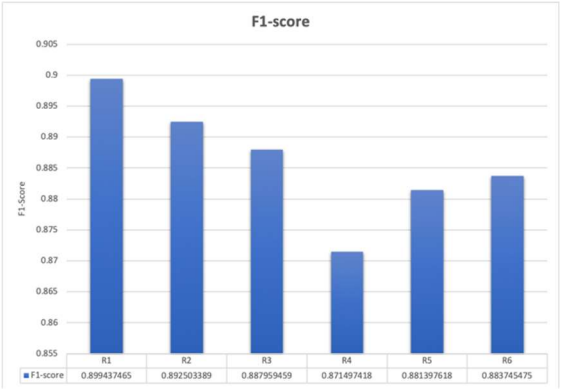

Figure 24 Our Model Without Our Sorting F1- Score For All Roughness Classes

As shown in the *Figure* ***24***, our sub model of showing the pattern without sorting the images has shown very strong results in F1-Score of get degree of roughness, as all the classes were classify with an f1-score is over 87%, especially in classify the lowest rough class, which is class No. 1, with a result of 89.94\% its almost 90\%, and the lowest value is class No. 4 with F1-Score value is 87.14\%

4.4 Comparisons

As shown in ***Table 4***, The proposed model is utilized with some general models. It was discovered that the outcomes of generic models were significantly improved by our proposed model.

These are excellent outcomes and evidence of the strength of our model, since our proposed model increased the accuracy by about 12\%.

Table 4 Comparison of All Results Between Our Model, Default CNN And Our Model Without Our Sorting Images.

Result Model	***Accuracy***	***Precision***	***Recall***	***F1-Score***
Our Whole Model	91.94%	92.75%	93.28%	93.01%
Default CNN	79.96%	79.83%	80.71%	80.26%
Our Model Without Sorting	88.29%	88.36%	88.88%	88.61%

Table 5 Comparison Between Models

Model	**Accuracy**
default Vgg16	79.63%
default resnet 50	77.85%
default Inceptionv3	76.48%
Vgg16 with our update	91.94%
resnet50 with our update	89.81%
Inceptionv3 with our update	88.37%

As shown in *Table* ***5***, We have compared our model with a set of widely used models in this context. The outcomes demonstrate how much better our model is than another models. Our model's with VGG16 score of 91.94% was much higher than the score of 79.63% obtained by VGG16 without the modification we made. It is also evident that the accuracy of each model was significantly impacted when our adjustment was added. Inceptionv3, for instance, increased from 76.48% to 88.37%.

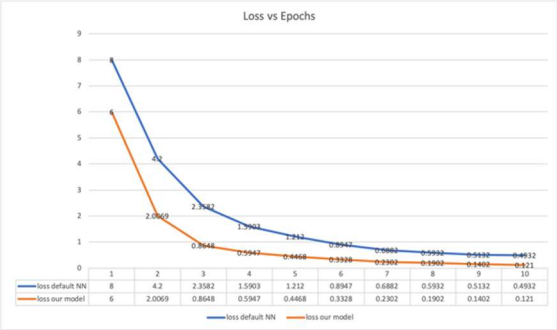

Figure 25 Loss Vs. Epoch Between VGG16 Without Our Modification And VGG16 With Our Modification.

As shown in *Figure* ***25***, where our model clearly deviates from the general model and reaches stability in a loss way, and this demonstrates both the power of our model and how quickly the model is approaching stability.

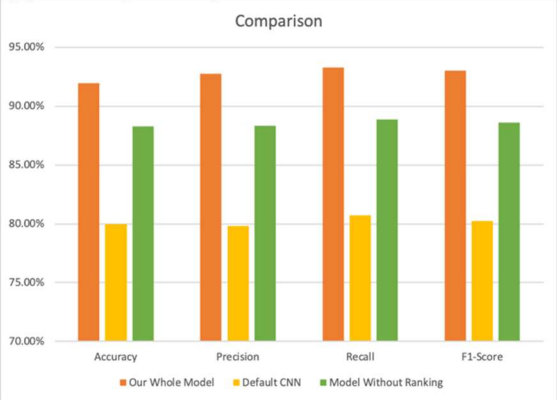

Figure 26 Chart Comparison Of All Results Between Our Model, Default CNN And Our Model Without Our Sorting Images.

As shown in the graph of *Figure* ***26***, when we compared our model to both the default model and our model without image sorting, we were able to clearly see that our model performed better than the general model across all four criteria, yielding the best overall result.

Journal of Theoretical and Applied Information Technology
15th July 2024. Vol.102. No. 13

ISSN: 1992-8645 www.jatit.org E-ISSN: 1817-3195

Table 6 Comparison Between Our Model And Different Technique In Clustering

Result Model	Accuracy	Precision	Recall	F1-Score
Our Model (VGG16)	91.94%	92.75%	93.28 %	93.01%
VGG16 with Random KMeans	80.74%	80.41%	79.06 %	79.73%
VGG16 with random KMeans with FreeDman-Diaconis	82.92%	87.52%	86.17 %	86.84%
VGG16 with KMeans with spikes without FreeDman-Diaconis	89.02%	88.97%	89.07 %	89.02%
VGG16 with Kmediods	77.82%	76.18%	74.95 %	75.56%

As shown in *Table* **6**, it compares several clustering techniques and demonstrates that our model gives the best results because it reduces a particular number of centroids.

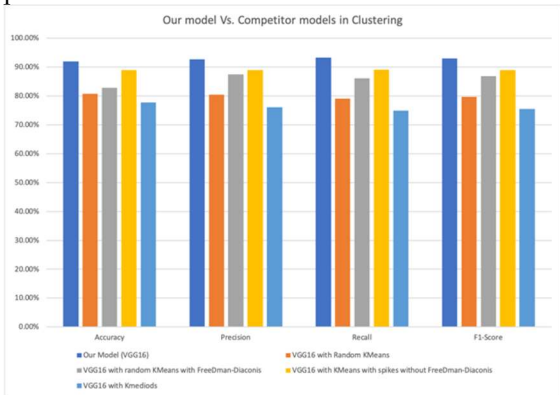

Figure 27 Chart of result of Accuracy, Precision, Recall and f1-score for Our model Vs. Competitor models in Clustering

The graph in *Figure* ***27*** shows the power of our approach and the outcome of other methods in clustering. The accuracy average was 91.94%, which is the highest of all the models and shows the power of combining the GLSZM Features spikes model with FreeDman-Diaconis to obtain a value of K.

Table 7 comparison between our model and different technique in texture classification on feature extraction with VGG16

Model Result	Accuracy	Precision	Recall	F1-Score
Our Model (VGG16)	91.94%	92.75%	93.28 %	93.01%
VGG16 with lbp	82.64%	82.65%	81.98 %	82.31%
VGG16 with edge detection	81.74%	82.55%	82.08 %	82.31%
VGG16 with Gabor Pattern	83.11%	81.92%	82.45 %	82.18%
VGG16 with Normal Histogram	82.02%	81.83%	81.36 %	81.59%

As shown in *Table 7* ,compares several techniques for texture classification on feature extraction using VGG16; the results indicate that our model performs best due to its high accuracy, precision, and recall, which are derived from extracting feathers in multiple directions.

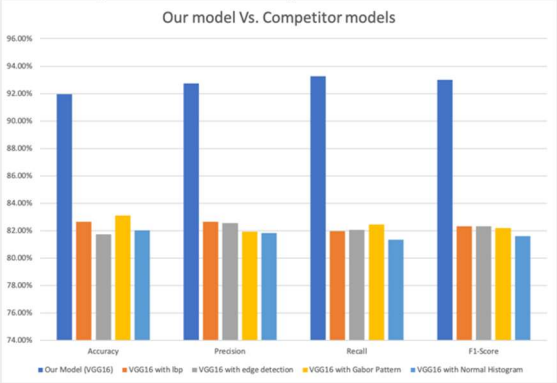

Figure 28 Chart of result of Accuracy, Precision, Recall and f1-score for Our whole model Vs. Competitor models in classification

The graph in Figure 28 demonstrates the power of our model and the outcome for other different models in the classification. The overall accuracy was 91.94%, which is the best outcome compared to all other models. This indicates the ability to combine the GLSZM approach with passion with deep rage to achieve the desired outcome.

Table 8 Comparison between Color Spaces

Color Space	Accuracy
LAB	91.94%
RGB	87.63%

Because the LAB color space is perceptual, outcomes using LAB have higher accuracy compared to outcomes using RGB, as Table 8 demonstrates.

5. CONCLUSION

In this paper, our contribution is to establish a new technique and model for finding, classifying and Ranking road roughness, by using the drone to take images to classify street roughness. The key to this algorithm's success or failure is determining the optimal K for the K-means clustering algorithm, which is determined by using the Gray Level Size Zone Matrix (GLSZM). In order to determine the cumulative likelihood of occurrence of the given pixel pairs, we extracted the SZV and ZP features of GLSZM in our study. These two features experience spikes. These spikes are calculated and assigned a K-value. The image might be divided into segments using K-means clustering and the computed K. Following that, and before transmitting the images to CNN for classification, another contribution we make is image sorting using GLSZM features with FreeDman-Diaconis to reduce the diversity of GLSZM features and goodness to fit technique to obtain the closest images. The outcomes showed our algorithm's effectiveness and showed its accuracy was 91.94%.

Here we conclude that our model was able to show the pattern with excellent accuracy, and this in turn leads to monitoring and updating the roads streets with the lowest costs, the best performance, and the best results under different circumstances.

In future work, we can apply our model in net of neural network, to study the roads from multi views to more accurate value.

REFRENCES:

[1] Abeygunawardhana, C., R. M. K. Sandamal, and H. R. Pasindu. "Identification of the Impact on Road Roughness on Speed Patterns for Different Roadway Segments." 2020 Moratuwa Engineering Research Conference (MERCon). 2020. 425–430.

[2] Alatoom, Yazan Ibrahim, and Turki I. Al-Suleiman. "Development of pavement roughness models using Artificial Neural Network (ANN)." International Journal of Pavement Engineering (Taylor & Francis), 2022: 1–16.

[3] Muniz de Farias, M., & de Souza, R. O. Correlations and analyses of longitudinal roughness indices. Road Materials and Pavement Design, 10(2) (2009), 399-415.

[4] Bajic, Milena, Shahrzad M. Pour, Asmus Skar, Matteo Pettinari, Eyal Levenberg, and Tommy Sonne Alstrøm. "Road Roughness Estimation Using Machine Learning." arXiv preprint arXiv:2107.01199, 2021.

[5] Cabral, Frederico Soares, Mateus Pinto, Fernao A. L. N. Mouzinho, Hidekazu Fukai, and Satoshi Tamura. "An automatic survey system for paved and unpaved road classification and road anomaly detection using smartphone sensor." 2018 IEEE International Conference on Service Operations and Logistics, and Informatics (SOLI). 2018. 65–70.

[6] Cao, Minh-Tu, Quoc-Viet Tran, Ngoc-Mai Nguyen, and Kuan-Tsung Chang. "Survey on performance of deep learning models for detecting road damages using multiple dashcam image resources." Advanced Engineering Informatics (Elsevier) 46 (2020): 101182.

[7] Cech, Jan, Tomas Hanis, Adam Kononisky, Tomas Rurtle, Jan Svancar, and Tomas Twardzik. "Self-supervised learning of camera-based drivable surface roughness." 2021 IEEE Intelligent Vehicles Symposium (IV). 2021. 1319–1325.

[8] Chen, Shong-Loong, Chun Lin, Chao-Wei Tang, and Hsin-Ang Hsieh. "Evaluation of Pavement Roughness by the International Roughness Index for Sustainable Pavement Construction in New Taipei City." Sustainability (Multidisciplinary Digital Publishing Institute) 14 (2022): 6982.

[9] Chou, C. "Pilot Project for Development of Pavement Performance Measurement Equipment." Institute of Transportation, Ministry ofTransportation and Communications: Taipei, Taiwan ISBN 986-00-2276-3 (2005).

[10] Daraghmi, Yousef-Awwad, Tsung-Hsiang Wu, and Tsì-Uí İk. "Crowdsourcing-Based Road Surface Evaluation and Indexing." IEEE Transactions on Intelligent Transportation Systems 23 (2022): 4164-4175.

[11] Dong, Xiaodong, Ping Lou, Junwei Yan, and Jiwei Hu. "A detection method for pavement roughness with binocular vision." Eleventh International Conference on Graphics and Image Processing (ICGIP 2019). 2020. 613–619.

[12] Du, Yuchuan, Ning Pan, Zihao Xu, Fuwen Deng, Yu Shen, and Hua Kang. "Pavement distress detection and classification based on YOLO network." International Journal of Pavement Engineering (Taylor & Francis) 22 (2021): 1659–1672.

[13] Dung, Cao Vu, and others. "Autonomous concrete crack detection using deep fully convolutional neural network." Automation in Construction (Elsevier) 99 (2019): 52–58.

[14] Gopalakrishnan, Kasthurirangan, Siddhartha K. Khaitan, Alok Choudhary, and Ankit Agrawal. "Deep convolutional neural networks with transfer learning for computer vision-based data-driven pavement distress detection." Construction and building materials (Elsevier) 157 (2017): 322–330.

[15] Hadjidemetriou, Georgios M., and Symeon E. Christodoulou. "Vision-and entropy-based detection of distressed areas for integrated pavement condition assessment." Journal of Computing in Civil Engineering (American Society of Civil Engineers) 33 (2019): 04019020.

[16] Ishtiak, Taoseef, Sajid Ahmed, Mehreen Hossain Anila, and Tanjila Farah. "A Convolutional Neural Network Approach for Road Anomalies Detection in Bangladesh with Image Thresholding." 2019 Third World Conference on Smart Trends in Systems Security and Sustainablity (WorldS4). 2019. 376–382.

[17] Janani, L., V. Sunitha, and Samson Mathew. "Influence of surface distresses on smartphone-based pavement roughness evaluation." International Journal of Pavement Engineering (Taylor & Francis) 22 (2021): 1637–1650.

[18] Jeong, Jong-Hyun, Hongki Jo, and Gregory Ditzler. "Convolutional neural networks for pavement roughness assessment using calibration-free vehicle dynamics." Computer-Aided Civil and Infrastructure Engineering (Wiley Online Library) 35 (2020): 1209–1229.

[19] Kumar, Pankaj, and Eduard Angelats. "AN AUTOMATED ROAD ROUGHNESS DETECTION FROM MOBILE LASER SCANNING DATA." International Archives of the Photogrammetry, Remote Sensing & Spatial Information Sciences 42 (2017).

[20] Lin, Jyh-Dong, Jyh-Tyng Yau, and Liang-Hao Hsiao. "Correlation analysis between international roughness index (IRI) and pavement distress by neural network." 82nd Annual Meeting of the Transportation Research Board. 2003. 1–21.

[21] Liu, Chiu, and Robert Herman. "Road profiles, vehicle dynamics, and human judgment of serviceability of roads: Spectral frequency domain analysis." Journal of transportation engineering (American Society of Civil Engineers) 124 (1998): 106–111.

[22] Liu, Qinghua, Lu Sun, Alain Kornhauser, Jiahui Sun, and Nick Sangwa. "Road roughness acquisition and classification using improved restricted Boltzmann machine deep learning algorithm." Sensor Review (Emerald Publishing Limited), 2019.

[23] Mandal, Vishal, Lan Uong, and Yaw Adu-Gyamfi. "Automated road crack detection using deep convolutional neural networks." 2018 IEEE International Conference on Big Data (Big Data). 2018. 5212–5215.

[24] Marinello, Francesco, Andrea Rosario Proto, Giuseppe Zimbalatti, Andrea Pezzuolo, Raffaele Cavalli, and Stefano Grigolato. "Determination of forest road surface roughness by Kinect depth imaging." Annals of Forest Research 60 (2017): 217–226.

[25] Sabha, Muath, and Muhammed Saffarini. "Selecting optimal k for K-means in image segmentation using GLCM." Multimedia Tools and Applications (2023): 1-17.

[26] Muniz de Farias, Márcio, and Ricardo O. de Souza. "Correlations and analyses of longitudinal roughness indices." Road Materials and Pavement Design (Taylor & Francis) 10 (2009): 399–415.

[27] Ouma, Yashon O., and Michael Hahn. "Wavelet-morphology based detection of incipient linear cracks in asphalt pavements from RGB camera imagery and classification using circular Radon transform." Advanced Engineering Informatics (Elsevier) 30 (2016): 481–499.

[28] RAMOS-ROMERO, Carlos, and César ASENSIO. "Asphalt-surface defects detection, based on tyre/road noise analysis and geo-processing." Proceedings of the International Congress on Acoustics. n.d.

[29] Saplioglu, Meltem, Ayse Unal, and Melek Bocek. "Detection of critical road roughness sections by trend analysis and investigation of driver speed interaction." Frontiers of Structural and Civil Engineering (Springer) 16 (2022): 515–532.

[30] Sarker, M. M., S. A. Hadigheh, and D. Dias-da-Costa. "Stereoscopic modelling and monitoring of roughness in concrete pavements." In ACMSM25, 635–644. Springer, 2020.

[31] Tan, Yumin, and Yunxin Li. "UAV photogrammetry-based 3D road distress detection." ISPRS International Journal of Geo-Information (MDPI) 8 (2019): 409.
[32] Thilak, Ram, Jeet Mehta, Vivikt Pharle, Chaturi Rajapur, Sabina Borah, and others. "Evaluation of Pavement Roughness Using Smartphones." 2021 IEEE International Conference on Computation System and Information Technology for Sustainable Solutions (CSITSS). 2021. 1–7.
[33] Valikhani, Alireza, Azadeh Jaberi Jahromi, Samira Pouyanfar, Islam M. Mantawy, and Atorod Azizinamini. "Machine learning and image processing approaches for estimating concrete surface roughness using basic cameras." Computer-Aided Civil and Infrastructure Engineering (Wiley Online Library) 36 (2021): 213–226.
[34] Guillaume Thibault; Bernard Fertil; Claire Navarro; Sandrine Pereira; Pierre Cau; Nicolas Levy; Jean Sequeira; Jean-Luc Mari. “Texture Indexes and Gray Level Size Zone Matrix. Application to Cell Nuclei Classification”. Pattern Recognition and Information Processing (2009) (PRIP): 140-145.
[35] D. Freedman & P. Diaconis (1981) “On the histogram as a density estimator: L2 theory”. Probability Theory and Related Fields 57 (4): 453-476.
[36] Massey Jr, Frank J. "The Kolmogorov-Smirnov test for goodness of fit." Journal of the American statistical Association 46, no. 253 (1951): 68-78.